UNIVERSIDADE DO VALE DO ITAJAÍ
ENGENHARIA DE COMPUTAÇÃO
FABIO IVO PEREIRA DE OLIVEIRA JUNIOR

SISTEMAS ROBÓTICOS – M2

Relatório apresentado como requisito parcial para a obtenção da M2 da disciplina de Sistemas Robóticos do curso de Engenharia de Computação pela Universidade do Vale do Itajaí da Escola Politécnica.

Prof. Alejandro Rafael G. Ramirez

Itajaí
2023

M2. Esta lista vale como atividade complementar da M2.

1.Em relação ao manipulador cilíndrico descreva as transformações (movimentos) dessa estrutura.

a.Replique a seguinte configuração no RoboAnalyzer e copie o movimento resultante do robô (animação que aparece na tela). Observação: simule os movimentos com a opção ‘trace end efector’ ativa.

b. A partir da simulação, que foi possível observar em relação aos movimentos do efetuador (volume de trabalho)?

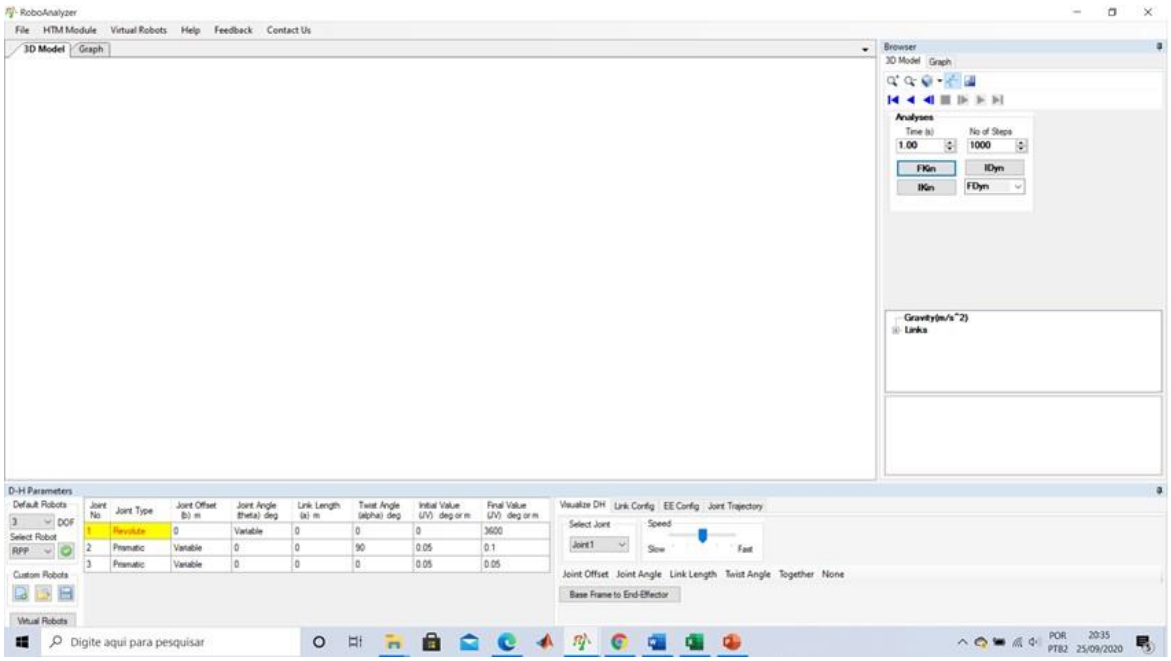

Resposta: Nosso sistema de coordenadas começa com Z0, localizado na origem, estabelecendo a direção da primeira junta rotativa, onde a rotação em relação a Z0 é expressa pela variável "theta1".

Z1 é um sistema de coordenadas adicional, situado a uma distância "e1" do sistema X0, Y0, Z0, apontando na direção do movimento linear da primeira junta prismática em relação a Z2, representado pela variável "D1".

E encontramos o sistema Z2, localizado na segunda junta prismática, apontando para a extremidade do braço. O movimento linear da segunda junta prismática em relação a Z3 é descrito pela variável "D2".

A junta J1 permite rotação contínua, permitindo que o efetor assuma várias orientações. Por outro lado, as juntas prismáticas J2 e J3 possibilitam o movimento linear ao longo de um eixo no espaço 3D, permitindo que o efetor se mova em várias direções. Essa combinação de movimentos rotacionais e lineares permite ao robô alcançar diversas posições e orientações no espaço 3D.

Essa adaptabilidade é de suma importância, pois capacita o robô a executar tarefas complexas em diversas aplicações, como montagem, manipulação de objetos e outras aplicações. A capacidade de se adequar a diferentes requisitos de tarefas e desempenhar várias funções com eficácia é uma característica essencial do robô.

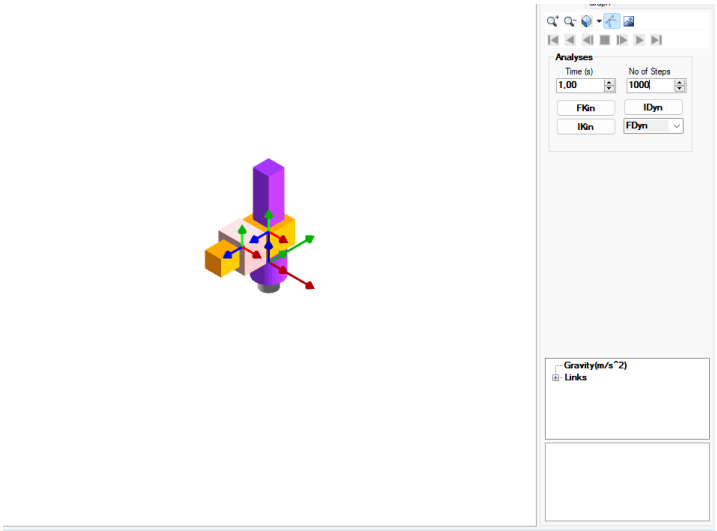
Analyses
Time (s)
1,00
No of Steps
1000
FKin
IDyn
IKin
FDyn
Gravity(m/s^2)
Links
D-H Parameters
Default Robots
3
DOF
Select Robot
RPP
Custom Robots
Virtual Robots
Joint No
Joint Type
Joint Offset (b) m
Joint Angle (theta) deg
Link Length (a) m
Twist Angle (alpha) deg
Initial Value (JV) deg or m
Final Value (JV) deg or m
1 Revolute 0 Variable 0 0 0 3600
2 Prismatic Variable 0 0 90 0,05 0,1
3 Prismatic Variable 0 0 0 0,05 0,05
Visualize DH
Link Config
EE Config
Select Joint
Joint1
Speed
Slow
Joint Offset
Joint Angle
Base Frame to End-Effector

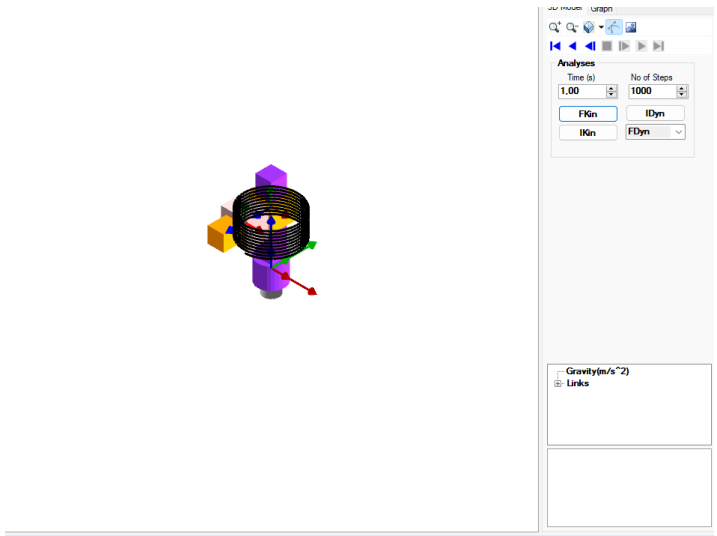
Analyses
Time (s)
1,00
No of Steps
1000
FKin
IDyn
IKin
FDyn
Gravity(m/s^2)
Links
D-H Parameters
Default Robots
3
DOF
Select Robot
RPP
Custom Robots
Virtual Robots
Joint No
Joint Type
Joint Offset (b) m
Joint Angle (theta) deg
Link Length (a) m
Twist Angle (alpha) deg
Initial Value (JV) deg or m
Final Value (JV) deg or m
1 Revolute 0 Variable 0 0 0 3600
2 Prismatic Variable 0 0 90 0,05 0,1
3 Prismatic Variable 0 0 0 0,05 0,05
Visualize DH
Link Config
EE Config
Select Joint
Joint1
Speed
Slow
Joint Offset
Joint Angle
Base Frame to End-Effector

2.Em relação ao manipulador esférico descreva as transformações (movimentos) dessa estrutura.

a.Replique a seguinte configuração no RoboAnalyzer e copie o movimento resultante do robô (animação que aparece na tela). Observação: simule os movimentos com a opção trace end efector ativa.

b. A partir da simulação, que foi possível observar em relação aos movimentos do efetuador (volume de trabalho)?

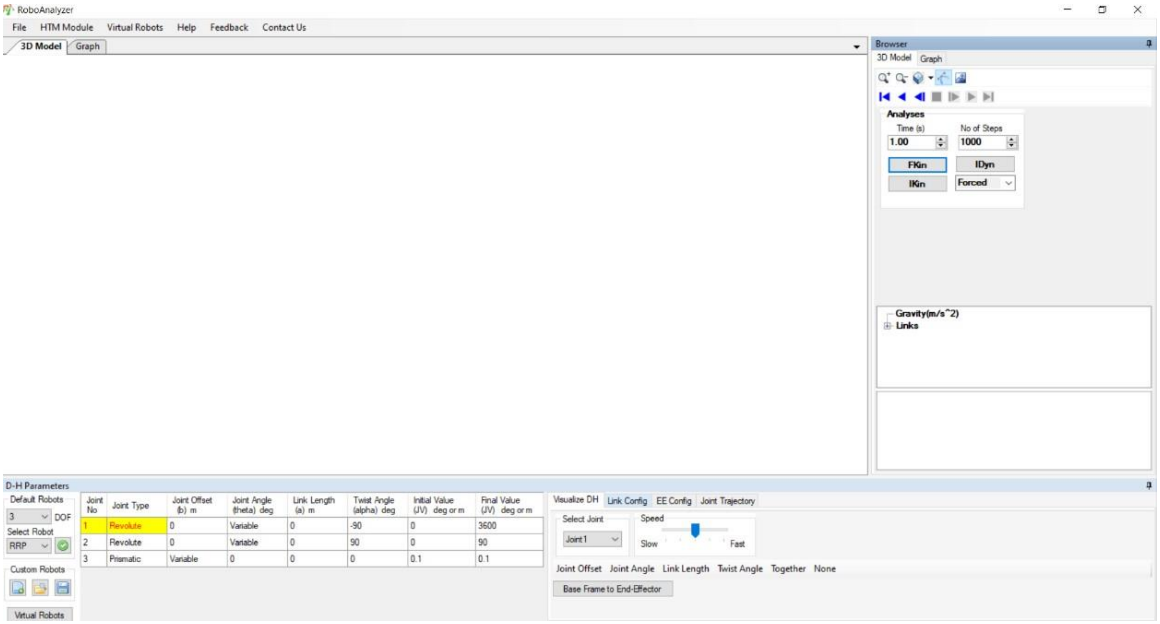

Respota: Junta J1: Localizada na base do manipulador, a junta J1 tem a capacidade de girar em torno de um eixo vertical. Isso permite ao manipulador realizar movimentos horizontais e apontar em diversas direções.

Junta J2: A junta J2, que segue a J1, pode girar em um eixo horizontal perpendicular à direção da junta J1. Essa capacidade permite ao manipulador alcançar diferentes alturas, movendo o efetuador para cima ou para baixo.

Junta J3: A junta J3, localizada entre as juntas J2 e J4, desempenha um papel vital no movimento ao longo do eixo radial. Isso possibilita ao efetuador se movimentar para dentro ou para fora em relação ao ponto central da junta J1, controlando, assim, a distância entre o efetuador e a base.

Junta J4: A junta J4, também situada em um eixo horizontal, permite ao efetuador final girar em torno de um eixo vertical. Esta junta é responsável por ajustar o ângulo de inclinação (pitch) do efetuador.

Essas transformações nas juntas possibilitam ao manipulador esférico realizar movimentos complexos no espaço tridimensional, concedendo-lhe a capacidade de controlar tanto sua orientação quanto sua posição. A precisão cartesiana deste manipulador é diretamente influenciada pelas configurações específicas das juntas e pelo controle preciso dos ângulos das juntas para atingir as coordenadas desejadas no espaço cartesiano.

A simulação revelou que o movimento do efetuador do robô assemelha-se a uma cúpula tridimensional no espaço. Esse movimento complexo é resultado da interação das configurações das juntas J1, J2 e J3, conforme explicado anteriormente. O espaço de trabalho deste arranjo específico do robô é definido por esta trajetória em forma de cúpula, descrevendo as posições e orientações que o efetuador pode atingir durante a simulação.

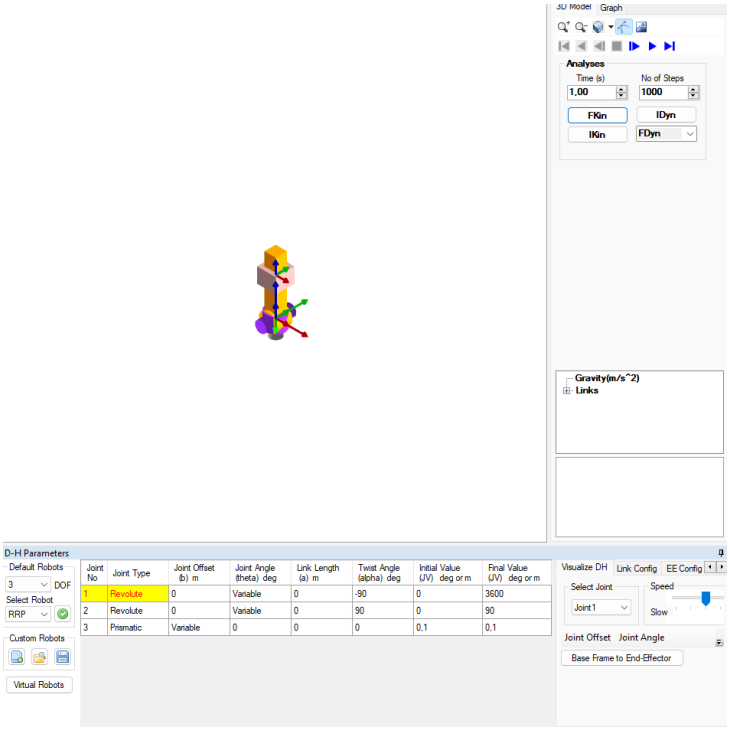

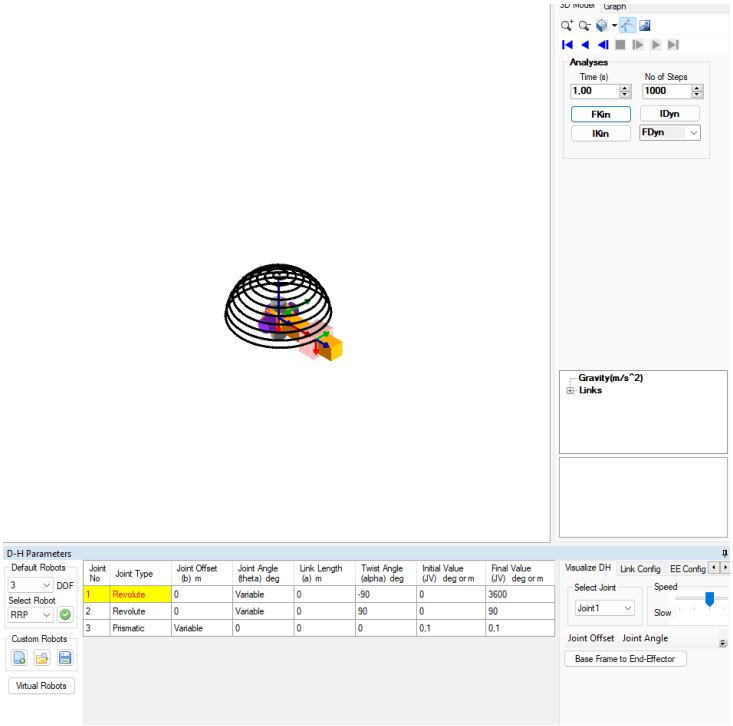

3.Realize um procedimento similar no RoboAnalyzer para o manipulador SCARA e realize o print da animação (após finalizada) dos movimentos com o recurso trace ativo. Observando que, nesse caso, a matriz de parâmetros resulta em:

Joint No	Joint Type	Joint Offset (b) m	Joint Angle (theta) deg	Link Length (a) m	Twist Angle (alpha) deg
1	Revolute	0.05	Variable	0.08	0
2	Revolute	0.05	Variable	0.08	180
3	Prismatic	Variable	90	0	0

a. A partir da simulação que podemos afirmar em relação ao volume de trabalho desse manipulador? Observação: vocês devem definir os ângulos e deslocamentos (iniciais e finais) da simulação.
b. Analisando todas as estruturas cinemáticas estudadas em aulas, qual, na sua opinião, é a mais simples? E qual a mais versátil e mais usada? Justifique a resposta.

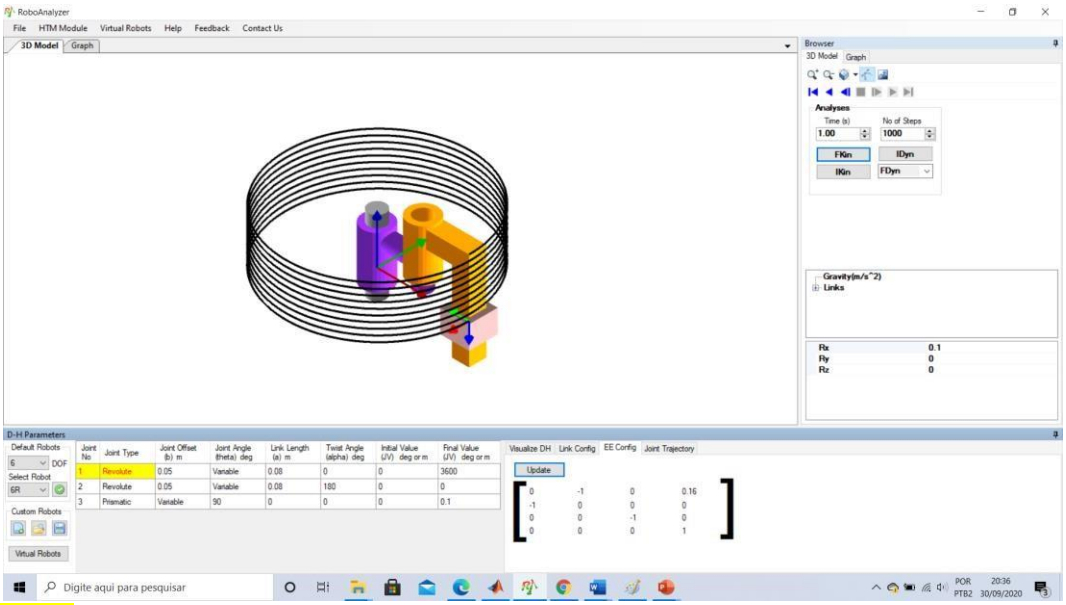

Resposta:

Tipos de Juntas: O manipulador SCARA é configurado com diferentes tipos de juntas. As juntas J1 e J2 são revolutas, permitindo rotação, enquanto a junta J3 é prismática, permitindo movimento linear.

Configuração Inicial e Final: Começando com a configuração inicial, a junta J1 é posicionada a 0 graus, a junta J2 também está a 0 graus, e a junta J3 tem um deslocamento inicial de 0.1 unidades de medida. Na configuração final da simulação, a junta J1 atinge 360 graus, a junta J2 permanece em 0 graus, e a junta J3 mantém seu deslocamento em 0.1 unidades de medida.

Espaço de Trabalho: A capacidade de rotação da junta J1 desempenha um papel fundamental na determinação do espaço de trabalho do manipulador SCARA. Essa característica oferece uma ampla gama de orientações angulares para o efetuador. Em contraste, o movimento linear da junta J3 contribui de forma mais restrita para o deslocamento linear do efetuador.

Comparando Estruturas Cinemáticas: No campo da robótica, uma variedade de estruturas cinemáticas é explorada, e o SCARA se destaca por sua notável simplicidade. Composta por três graus de liberdade (DOF) e configurada como RRP (Revolute-Revolute-Prismatic), essa estrutura consiste em duas juntas rotativas e uma junta prismática. Sua simplicidade é evidente na disposição direta das juntas e na facilidade de controle que oferece.

Versatilidade da Estrutura 6-DOF: Quando se trata de escolher uma estrutura cinemática mais versátil, muitas vezes é considerada a configuração de 6 graus de liberdade (6-DOF) com um arranjo RRRRRR (Revolute-Revolute-Revolute-Revolute-Revolute-Revolute). Essa configuração permite uma ampla gama de movimentos em todas as direções, tornando-a popular na robótica industrial para tarefas como montagem, soldagem e manipulação.

Seleção da Estrutura Adequada: A escolha da estrutura robótica mais adequada depende de diversos fatores, como o ambiente de trabalho, as tarefas específicas a serem realizadas e os recursos disponíveis. Portanto, é essencial realizar uma avaliação cuidadosa antes de tomar a decisão final. Enquanto o SCARA encontra seu nicho em aplicações que exigem movimento predominantemente em um plano horizontal, como montagem precisa e tarefas de posicionamento, a estrutura 6-DOF RRRRRR continua sendo uma escolha flexível em vários cenários.

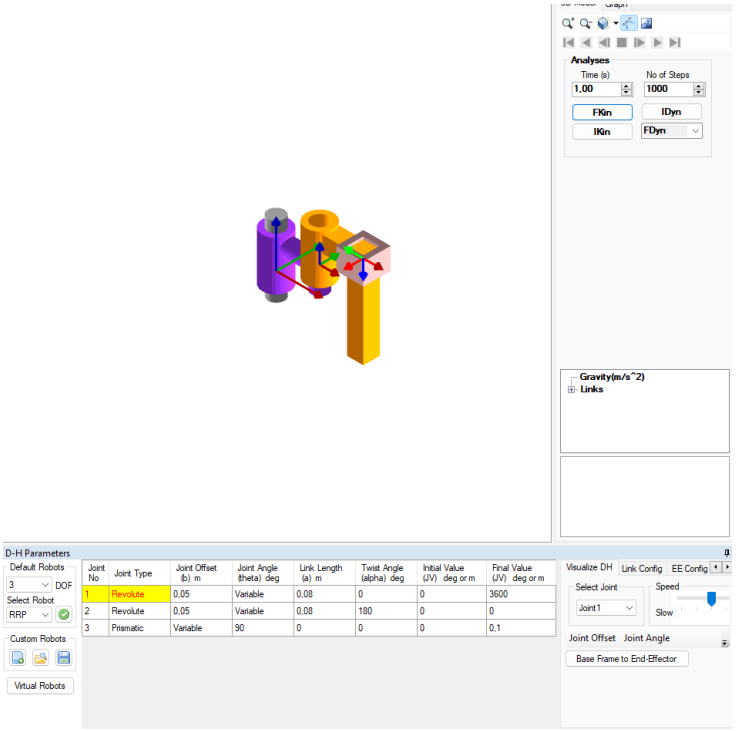

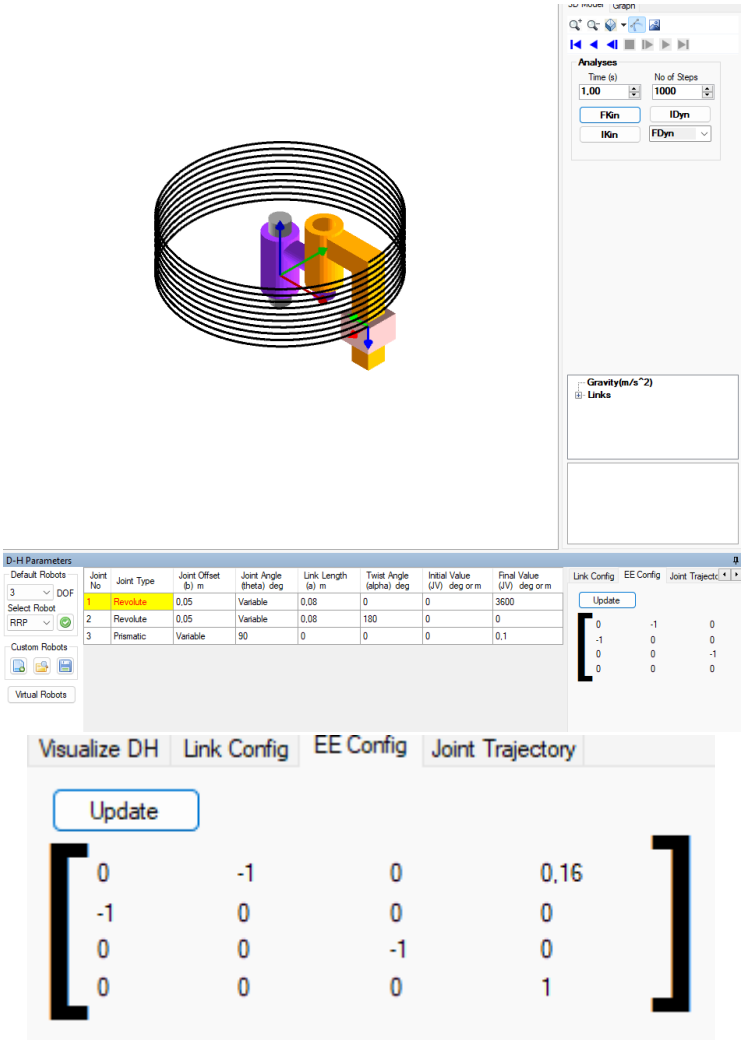

4. Ler as duas primeiras páginas do artigo Kinematic Control of an Articulated Minimally Invasive Surgical Robotic Arm e usar a Tabela 1 como referência para modelar o robô usando o RoboAnalyzer (pode ser também usado o Matlab). Este artigo foi apresentado em IEEE First International Conference on Power Electronics, Intelligent Control and Energy Systems. Delhi Technological University. 2016.

Considerar L1 = L2 = 0.2, e L3 = 0.05.

Reparem que o artigo cita a metodologia que estamos estudando:

J. Denavit and R. S. Hartenberg, “A kinematic notation for lower-pair mechanisms based on matrices.” Trans. of the ASME. Journal of Applied Mechanics.

Neste exercício deverá ser incluído no relatório o print da tela usando as seguintes variações dos ângulos theta.

Initial Value (JV) deg or m	Final Value (JV) deg or m
0	180
0	60
0	60
0	180
0	180
0	3600

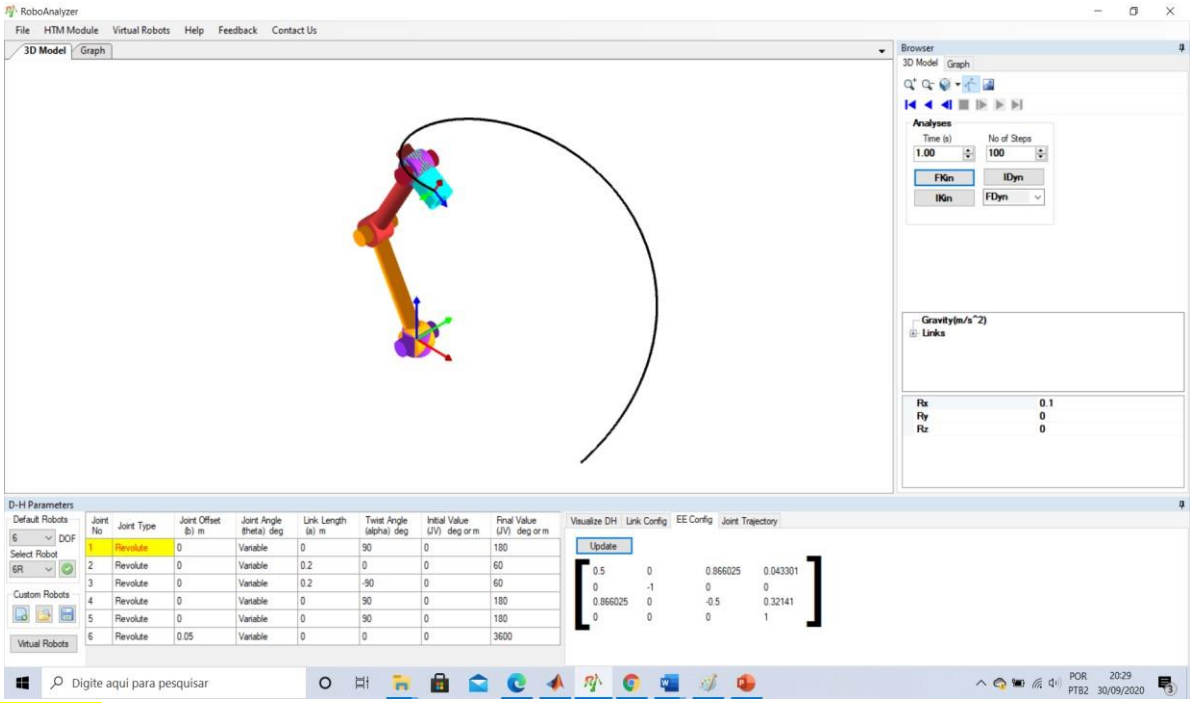

Resposta: O artigo "Kinematic Control of an Articulated Minimally Invasive Surgical Robotic Arm" explora a capacidade de um braço robótico articulado geral (GARA) realizar operações minimamente invasivas. O braço robótico é usado em cirurgias minimamente invasivas, onde ele entra no corpo do paciente através de uma porta, limitando a tradução do efetuador ao longo de dois eixos. A pesquisa visa realizar operações minimamente invasivas usando um braço robótico articulado convencional, independentemente de seu design, desde que apenas o elo final seja restrito.

A abordagem envolve transformações geométricas baseadas nas restrições no elo final, juntamente com relações cinemáticas obtidas por técnicas convencionais. Isso permite ao braço robótico realizar operações minimamente invasivas. O método é validado por meio de simulações, rastreando trajetórias planares e 3D

predefinidas. Os resultados mostram desvios médios nas trajetórias rastreadas da ordem de 10^-3 cm e erros médios absolutos na manutenção do centro de movimento remoto (RCM) na porta de cerca de 10^-15 cm.
O estudo demonstra que é possível que um GARA realize operações minimamente invasivas sem a necessidade de design especializado e com precisão suficiente. O artigo enfatiza que a capacidade de realizar cirurgias minimamente invasivas pode ser incorporada a braços robóticos articulados gerais, ampliando sua utilidade.
Em resumo, o artigo apresenta uma abordagem para permitir que braços robóticos articulados gerais realizem cirurgias minimamente invasivas de forma precisa e eficaz, sem a necessidade de alterações significativas em seu design.

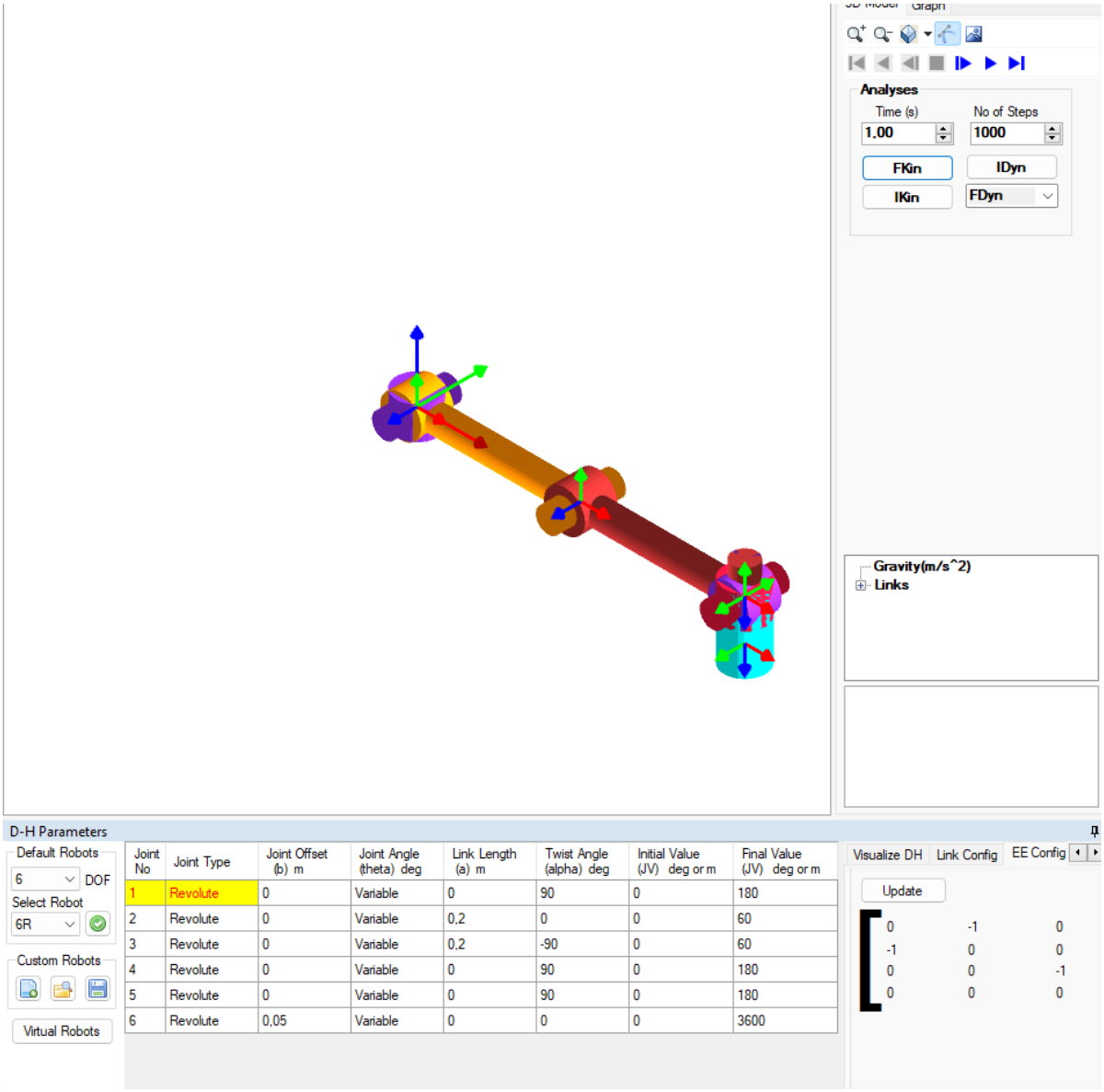

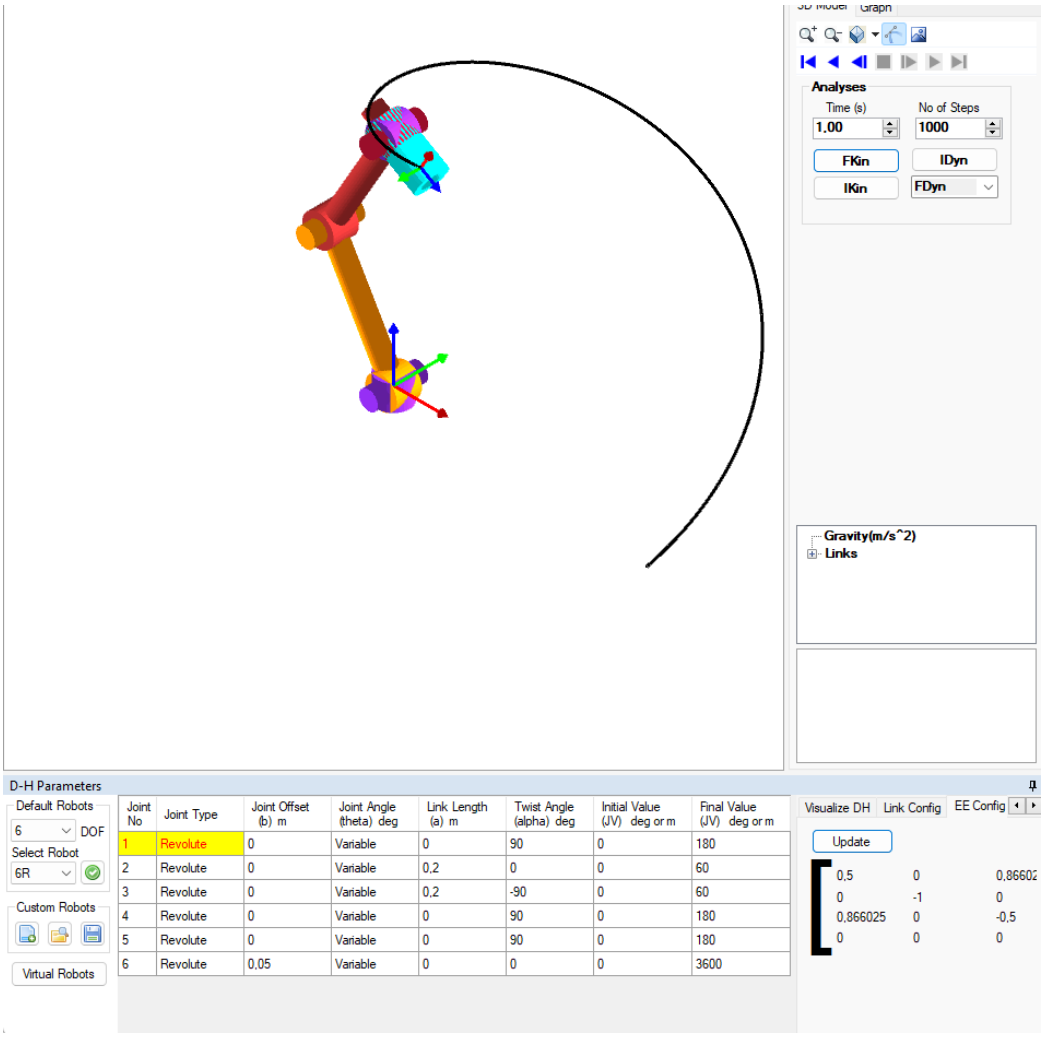
Graph
Analyses
Time (s)
No of Steps
1,00
1000
FKin
IDyn
IKin
FDyn
Gravity(m/s^2)
Links
D-H Parameters
Default Robots
6
DOF
Select Robot
6R
Custom Robots
Virtual Robots
Joint No
Joint Type
Joint Offset (b) m
Joint Angle (theta) deg
Link Length (a) m
Twist Angle (alpha) deg
Initial Value (JV) deg or m
Final Value (JV) deg or m
1 Revolute 0 Variable 0 90 0 180
2 Revolute 0 Variable 0,2 0 0 60
3 Revolute 0 Variable 0,2 -90 0 60
4 Revolute 0 Variable 0 90 0 180
5 Revolute 0 Variable 0 90 0 180
6 Revolute 0,05 Variable 0 0 0 3600
Visualize DH
Link Config
EE Config
Update
0,5 0 0,86602
0 -1 0
0,866025 0 -0,5
0 0 0

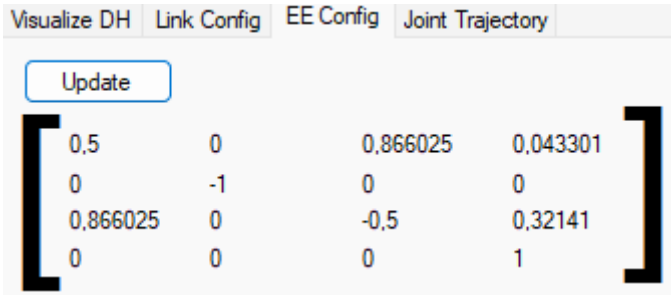
Visualize DH
Link Config
EE Config
Joint Trajectory
Update
0,5 0 0,866025 0,043301
0 -1 0 0
0,866025 0 -0,5 0,32141
0 0 0 1

Kinematic Control of an Articulated Minimally Invasive Surgical Robotic Arm

Surbhi Gupta, Sankho Turjo Sarkar, and Amod Kumar
Academy of Scientific and Innovative Research
CSIR-Central Scientific Instruments Organisation, India
Email: surbhig@csio.res.in

Abstract—The robotic arm used in minimally invasive surgery enters patient's body through a port which constrains its endeffector translation along two axes. We aim to achieve the minimally-invasive operations using a general articulated robotic arm (GARA). The algorithm is applicable to articulated robotic arm independent of its design; given only end-link is constrained. Geometric transformations based on the constraints acting on the end-link coupled with kinematic-relations obtained using conventional techniques, were used to drive a simulated 6DOF GARA for minimally-invasive operations. The method was verified by tracing predefined planar and 3D trajectories using this simulated arm. The mean deviation of the traced trajectories was of the order of 10^{-03}cm and the mean absolute error in maintaining remote center-of-motion (RCM) at the port was ~0 (< 10^{-15} cm). The proposed method enabled a GARA to perform minimally-invasive operations without specialized design and with sufficient accuracy.

Index Terms—Jacobian technique, kinematics, minimally invasive robotic arm, motion control.

I. Introduction

Minimally invasive robotic surgery [1], [2] provides the surgeon ability to perform surgical operations using minimally invasive techniques. The surgeon tele-operates minimally invasive robotic arm which enters the patient's body through ports placed at small incisions in the body surface. During such a surgery, only a surgical tool may access the operation area instead of the entire mechanism driving the tool. Using MIRA for surgeries provides cosmetic advantages, causes minimum trauma, reduced blood loss [3], [4] and postoperative pain [5] to the patient. However, most of the present MIRAs [6], [7] which have a remote center-of-motion (RCM) at the port, differ drastically in design from the existing industrial robotic manipulators [8]–[10] which work in open or unrestricted environment. We hypothesize that this change in design is not necessary to accomplish minimally invasive operations.

A fully-actuated articulated robotic arm can easily orient and place its tool at any desired location inside its reachable workspace by actuating its rotational joints. However, an arm operating as MIRA has a passive joint at the RCM. This RCM has fixed location on the patient's body surface, but is movable along the length of the end link, as the arm exhibits translation motion to enter or exit the body, i.e. it is fixed in the global reference frame but not in the local frame of the arm. The virtually pivoted operation through a port

978-1-4673-8587-9/16/$31.00

constrains the end-effector translation along two axes, leaving it with a maximum of four degrees of freedom (DoF) [11]. Hence, the MIRA should be able to maneuver its end-effector along the desired trajectories (achievable by the 4 DOFs) while maintaining its RCM at the port placed at the small incision. Various systems achieve this by using different types of mechanisms [12] or design changes viz. additional passive joints; double-parallelogram mechanism; parallel, serial or hybrid spherical mechanisms etc. Apart from lose of generality of the design, these mechanisms have several disadvantages, as summarized by Kim et al. [13]. Common problems posed by such mechanisms [14], [15] are: bulkiness and heaviness of the system, high chances of self or robot-robot collisions [16]. The RAVEN system [17] avoids these problems by using a 2link (C-arms), 3-DoF MIRA which considers a single revolute joint at shoulder and elbow each, leaving rest of the DoFs to the gripper's end. It also fixes the port position to the point where axes of rotation of all 3 joints intersect, thus restricting the user's freedom to choose port placement location. Several MIRAs use prismatic joints [18], [19] which are less desirable than revolute joints due to their bulkiness and mechanical complexity. Unlike formerly mentioned works, Michellin et al. [20] used Mitsubishi's PA-10, an industrial manipulator as a MIRA. However, they used computationally expensive optimization method to determine the elbow coordinates corresponding to the desired end-effector position, which provides approximate solution, and thus is not as accurate as an analytical solution. Hence, a general articulated robotic arm (GARA) of common design, using conventional kinematic analysis methods, and having minimally invasive operation abilities is most desirable. In this paper, we present kinematic equations mapping elbow position of a 6-DoF GARA to the joint angles and a transformation function between the elbow coordinates (external to the separating surface) and the end-effector coordinates (internal to the separating surface) to enable minimally invasive operations. Though the kinematics equations are derived by the conventional kinematic analysis method, the novelty lies in the transformation function which relates the elbow position to end-effector position such that the arm has a RCM at the port. Coupling both enables direct control of the end-effector by joint actuations. The derived transformation function is independent of the arm design, ruling out changes in mechanical design to convert a GARA into an MIRA. Also, this function coupled with derived kinematic relations provide the end effector with one translational and three rotational independent degrees of freedom, which is necessary and sufficient for tool maneuver during a minimally invasive surgery. As the Jacobian matrix is not rank-deficient and is a square matrix, we chose Jacobian inverse technique from the vast pool of algorithms [21]–[24] present for solving the inverse kinematics problem. The motion control algorithm based on derived kinematic relations and the mapping function is verified through simulation for tracking trajectories provided by planar and three-dimensional timed gesture data.

As MIRA is a slave arm, teleoperated by a surgeon using master control devices which do not suffer port constraints and provide only the desired trajectory information, any free hand movement trajectories would suffice for the validation. Hence, due to unavailability of the hand movement data from a minimally invasive surgical procedure, we used planar and 3D hand motion data from LIBRAS (Brazilian Sign Language) [25] and Auslan (Australian Sign Language) databases [26] available at the UCI repository [27].

II. Kinematics

In this section, we formulate forward and inverse kinematic relations to relate the position and orientation of the elbow of a 6-DoF GARA (Fig. 1) to its joint angles and couple it with a new transformation function to accomplish minimally invasive operations. The arm consists of three links connected serially by six revolute joints. We first transform the desired end-effector position to the arm elbow position, such that the arm's RCM is at the port $\mathbf{X}_p = (\ x_p \quad y_p \quad z_p\ )$ in global reference frame. However, in local frame, this RCM can move along the length of the end link. Since the displacement of the RCM along $\vec{L}_3$ in local frame would be equal to displacement of end-effector or elbow along $\vec{L}_3$ in global frame, desired elbow coordinates can be obtained using:

$$\mathbf{X}^{des} \quad L_3*(\mathbf{X}_{end}-\mathbf{X}_p)$$

$$^{des}\ \alpha_{elb}^{des} = \arccos\left(\frac{\mathbf{X}_{end}^{des}-\mathbf{X}_p}{\|\mathbf{X}_{end}^{des}-\mathbf{X}_p\|}\right)$$

$$z_{elb} = L_1 s_2 + L_2 s_{23}$$

$$\left(s \quad c\ s\ s \quad -c \quad c\ s\ +s \quad s\ c\right)$$

$$\mathbf{X}_{deselb} = \quad end - \quad \|\mathbf{X}_{desend}-\mathbf{X}_p\| \tag{1}$$

Here, $\mathbf{X}_{des_{elb}} = [x_{des_{elb}}, y_{elbdes}, z_{elbdes}]$ and $\alpha_{des_{elb}} = [\ \alpha_{elbdes}, \beta_{elbdes}, \gamma_{elbdes}\ ]$ are the desired elbow position and orientation vectors above the port corresponding to the desired end position $\mathbf{X}_{desend} = [\ x_{desend}, y_{enddes}, z_{enddes}\ ]$ in the end-effector workspace.

Then we can map joint angles to the elbow position and orientation using the widely known Denavit and Hartenberg (D-H) [28] convention. The D-H parameters for this arm is presented in Table I.

Forming the transformation matrix [29] for base to elbow using the D-H parameters, we can find the relations for position and orientation of elbow of the robotic arm as given in (2).

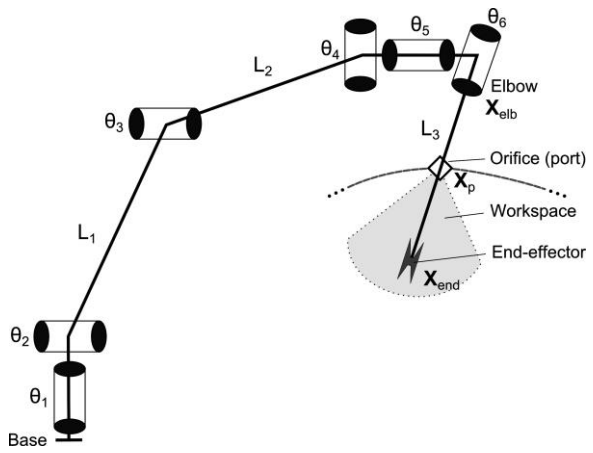

Fig. 1. The 6 DOF General Articulated Robotic Arm used to perform minimally invasive opertions. It consists of three links with length L_1, L_2 and L_3 connected serially by six revolute joints. θ_1 the base joint angle and θ_4 undergo yaw rotations; θ_2,θ_3 and θ_5, pitch and θ_6, roll .

Table I
D-H parameters table for the robotic arm

i	α	a	d	θ
1	90°	0	0	$\theta_1 + 90^\circ$
2	0°	L_1	0	θ_2
3	-90°	L_2	0	θ_3
4	90°	0	0	θ_4
5	90°	0	0	$\theta_5 + 90^\circ$
6	0°	0	L_3	θ_6

$$elb \qquad 1\ 1\ 2 \qquad 2\ 1\ 23$$

$$\alpha = \arctan \ \frac{23\ 4\ 5\ 6 \quad 23\ 5\ 6 \quad 23\ 4\ 6}{s_{23}c_4c_5+c_{23}s_5}$$

$$\beta = \arctan\left(\frac{s_{23}c_4s_5c_6-c_{23}c_5c_6-s_{23}s_4s_6}{s_{23}c_4s_5s_6-c_{23}c_5s_6+s_{23}s_4s_6} * sin\,(\alpha)\right)$$

$$\gamma = \arctan\left(\frac{-c_1c_{23}c_4s_5c_6-c_1s_{23}c_5c_6+c_1c_{23}s_4s_6+s_1c_4s_6}{s_1c_{23}c_4s_5c_6+c_1s_4s_5c_6+s_1s_{23}c_5c_6-s_1c_{23}s_4s_6+c_1c_4s_6}\right) \tag{2}$$

$$x_{elb} = -\ {}_1s_1c_2 - \ {}_2s_1c_{23}$$

$$y \quad = L\ c\ c\ + L\ c\ c \qquad L$$

$$L$$

Where, $s_i = sin(\theta_i)$, $c_i = cos(\theta_i)$, $s_{ij} = sin(\theta_i + \theta_j)$ and $c_{ij} = cos(\theta_i + \theta_j)$;$\alpha,\beta,\gamma$ represent the rotation of MIRA elbow about x,y,z axis, respectively, of global frame, and $[x_d\, y_d\, z_d]$ are the global position coordinates of MIRA elbow. The orientation of the end-effector would be same as that of the elbow. However, to ensure that the arm always passes through the port/incision, the position of the end-effector $\mathbf{X}_{end} = [x_{end}\, y_{end}\, z_{end}]$ should be calculated

$$\mathbf{X}_{end} = X_{elb} + \frac{L_3 * (\mathbf{X}_p - \mathbf{X}_{elb})}{\|\mathbf{X}_{elb} - \mathbf{X}_p\|} \tag{3}$$

The formulated position and orientation vectors $\mathbf{X}_{elb} =$

$[x_{elb}\ y_{elb}\ z_{elb}]$ and $\boldsymbol{\alpha} = \begin{bmatrix} \alpha & \beta & \gamma \end{bmatrix}$ of the arm elbow given in (2) are highly non-linear functions of joint variables, hence, finding inverse relations would be highly complex. However, it is well-established [24], [30] that working with rates rather than positions linearizes these relations. So if we make small changes in joint angles, we get:

$$4\mathbf{X}_{elb} = \mathbf{J}4\vartheta \tag{4}$$

The Jacobian matrix **J** is of the form:

$$\mathbf{J} = \begin{bmatrix} \frac{\delta f_1(\boldsymbol{\theta})}{\delta\theta_1} & \cdots & \frac{\delta f_1(\boldsymbol{\theta})}{\delta\theta_6} \\ \vdots & \ddots & \vdots \\ \frac{\delta f_6(\boldsymbol{\theta})}{\delta\theta_1} & \cdots & \frac{\delta f_6(\boldsymbol{\theta})}{\delta\theta_6} \end{bmatrix} \tag{5}$$

where, **J** is Jacobian matrix, $f_1(\vartheta), f_2(\vartheta), \cdots, f_6(\vartheta)$ are functions of joint space variables given in (2). The Jacobian matrix derived from (2) and (5) is given below, where, J_{ik} is the matrix element in i^{th} row and k^{th} column.

$$J_{11} = -L_1c_1c_2 - L_2c_1c_{23} \qquad J_{12} = L_1s_1s_2 + L_2s_1s_{23}$$
$$J_{21} = -L_2s_1c_{23} - L_1s_1c_2 \qquad J_{22} = -L_2c_1s_{23} - L_1c_1s_2$$
$$J_{13} = L_2s_1s_{23} \qquad J_{23} = -L_2c_1s_{23} \qquad J_{32} = L_1c_2 + L_2c_{23}$$
$$J_{31} = J_{41} = J_{14} = J_{24} = J_{34} = J_{15} = J_{25} = J_{35} = 0$$
$$J_{33} = L_2c_{23} J_{16} = J_{26} = J_{36} = J_{51} = 0$$
$$D_4 = (s_{23}c_4c_5 + c_{23}s_5)_2 + (s_{23}c_4s_5s_6 - c_{23}c_5s_6 + s_{23}s_4c_6)_2$$
$$J_{42} = J_{43} = \frac{c_4s_6 + s_4s_5c_6}{D_4}$$
$$J_{44} = \frac{s_{23}^2c_5c_6 - c_{23}s_{23}s_4s_6 + c_{23}s_{23}c_4s_5c_6}{D_4}$$
$$J_{45} = \frac{s_{23}^2c_4^2s_6 + c_{23}^2s_6 + s_{23}^2c_4s_4s_5c_6 - s_{23}c_{23}s_4c_5c_6}{D_4}$$
$$J_{46}^{'} = \frac{s_{23}^2c_4^2c_5s_5c_6 - s_{23}^2c_4s_4c_5s_6 - c_{23}^2c_5s_5c_6 - c_{23}s_{23}s_4s_5s_6}{D_4}$$
$$J_{46} = J_{46}^{'} + \frac{-c_{23}s_{23}c_4c_6\cos(2\theta_5)}{D_4}$$
$$K = s_{23}c_4s_5s_6 - c_{23}c_5s_6 + s_{23}s_4c_6$$
$$M = s_{23}c_4s_5c_6 - c_{23}c_5c_6 - s_{23}s_4s_6$$
$$Q = \arctan\left(\frac{K}{s_{23}c_4c_5 + c_{23}s_5}\right)$$
$$P = \frac{K}{K_5^2 + (s_{23}c_4s_5c_6 - c_{23}c_5c_6 - s_{23}s_4s_6)^2 * \sin^2(Q_5)}$$
$$J_{52} = J_{53} = P * \left\{\frac{s_4c_5s_Q}{K} + M * c_Q * \frac{c_4s_6 + s_4s_5c_6}{(s_{23}c_4c_5 + c_{23}s_5)^2 + K^2}\right\}$$
$$J_{54} = P * \left\{M * c_Q * \left(\frac{s_{23}^2c_5c_6 - c_{23}s_{23}s_4s_6 + c_{23}s_{23}c_4s_5c_6}{(s_{23}c_4c_5 + c_{23}s_5)^2 + K^2}\right) \cdots\right.$$
$$\left. \cdots + \left(\frac{-s_{23}^2s_4^2s_5 - s_{23}^2c_4^2s_5 + c_{23}s_{23}c_4c_5c_6^2 + c_{23}s_{23}s_4c_5s_5c_6s_6}{K}\right) * s_Q\right\}$$
$$J_{55} = P * \left\{\left(\frac{s_{23}^2c_4s_4c_5 + c_{23}s_{23}s_4s_5}{K}\right) * s_Q \cdots\right.$$
$$\left. \cdots + M * c_Q * \left(\frac{s_{23}^2c_4^2s_6 + c_{23}^2s_6 + s_{23}^2c_4s_4s_5c_6 - s_{23}c_{23}s_4c_5c_6}{(s_{23}c_4c_5 + c_{23}s_5)^2 + K^2}\right)\right\}$$
$$J_{56} = P * \left\{\left(\frac{-s_{23}^2s_4^2 - (s_{23}c_4s_5 - c_{23}c_5)^2}{K}\right) * s_Q + K * c_Q \cdots\right.$$
$$\cdots * \left(\frac{s_{23}^2c_4^2c_5s_5c_6 - s_{23}^2c_4s_4c_5s_6 - c_{23}^2c_5s_5c_6 - c_{23}s_{23}s_4s_5s_6}{(s_{23}c_4c_5 + c_{23}s_5)^2 + K^2}\right) \cdots$$
$$\left. \cdots * \left(\frac{-c_{23}s_{23}c_4c_6\cos(2\theta_5)}{(s_{23}c_4c_5 + c_{23}s_5)^2 + K^2}\right)\right\}$$
$$D_6 = c_{23}^2c_4^2s_5^2c_6^2 + s_{23}^2c_5^2c_6^2 + c_{23}^2s_4^2s_6^2 + c_1^2s_4^2s_5^2c_6^2$$
$$-2c_{23}^2c_4s_4s_5c_6s_6 - 2s_{23}c_{23}s_4c_5c_6s_6 + 2c_{23}c_4s_{23}c_5s_5c_6^2$$
$$+2s_1c_1c_{23}c_4s_4s_5^2c_6^2 + 2s_1c_1s_{23}s_4c_5s_5c_6^2$$
$$+2c_1^2c_4s_4s_5c_6s_6 - 2c_1s_1c_{23}s_4^2s_5c_6s_6$$

$$J_{61} = \frac{\begin{pmatrix} -2c_{23}^2c_4s_4s_5c_6s_6 - 2c_{23}s_{23}s_4c_5c_6s_6 \\ +2c_{23}s_{23}c_4c_5s_5c_6^2 + c_{23}^2c_4^2s_5^2c_6^2 + s_{23}^2c_5^2c_6^2 \\ +c_4^2s_6^2 + c_4s_4s_5c_6s_6 + c_{23}^2s_4^2s_6^2 \end{pmatrix}}{D_6}$$
$$J_{62} = \frac{\begin{pmatrix} c_{23}c_4c_5c_6s_6 - s_{23}c_4s_4s_6^2 + s_{23}c_4^2s_5c_6s_6 + \\ c_1^2s_{23}c_4s_4s_5^2c_6^2 + c_1^2c_{23}s_4c_5s_5c_6 + c_1^2s_{23}s_4^2s_5c_6s_6 \end{pmatrix}}{D_6}$$
$$J_{62} = J_{63}$$
$$J_{64} = \frac{\begin{pmatrix} -c_1^2c_{23}s_5^2c_6^2 - c_{23}c_4^2s_6^2 + c_1s_1s_5c_6s_6 - c_{23}s_4^2s_6^2 \\ -s_{23}s_4c_5c_6s_6 - c_1^2s_{23}c_4c_5s_5c_6^2 \end{pmatrix}}{D_6}$$
$$J_{65} = \frac{\begin{pmatrix} c_{23}c_4^2c_5c_6s_6 - c_1^2s_{23}s_4c_6^2 + c_1^2c_{23}s_4^2c_5c_6s_6 \\ +c_1s_1c_4s_4c_5c_6s_6 - s_{23}c_4s_5c_6s_6 \end{pmatrix}}{D_6}$$
$$J_{66} = \frac{-c_1^2c_{23}s_5 - s_{23}c_4c_5 - s_1^2c_{23}c_4^2s_5 - c_1s_1c_4s_4s_5}{D_6}$$

(6)

If the previous joint vector is known, then a change in the elbow position vector can be mapped to a new joint variable vector using (7):

$$\vartheta_{new} = \vartheta_{prev} + \mathbf{J}\text{-}14\mathbf{X}_{elb} \tag{7}$$

The complete motion control algorithm proposed is summarized in Algorithm (1).

Algorithm 1 Tracing a trajectory with minimal invasiveness

Given the desired trajectory to be tracked and incision point coordinates $\mathbf{X}_p$ for an MIRA with fixed link lengths $L = [L_1L_2L_3]$ and with initial joint-angle configuration ϑ_{start}:

1) $\vartheta_{new} := \vartheta_{start}$
2) For each $\mathbf{X}^{des}_{end} \in Trajectory$
   a) $\vartheta_{prev} := \vartheta_{new}$
   b) $X_{elbdes} \leftarrow (\mathbf{X}_{desend}; \mathbf{X}_p, L_3)$ from (1)
   c) $4\mathbf{X}_{elb} := \mathbf{X}_{deselb} - \mathbf{X}_{elb}$, where, $\mathbf{X}_{elb}$ is the current position and orientation of arm elbow.
   d) $J \leftarrow (\vartheta_{prev}; L)$ from (6)
   e) $4\vartheta \leftarrow (4\mathbf{X}_{elb}, J)$ from (7)
   f) New joint-angles vector $\vartheta_{new} := \vartheta_{prev} + 4\vartheta$,

---

III. Error Calculation

The objective of the proposed motion control algorithm is two-fold: firstly, the desired trajectory should be accurately tracked, and secondly, the end link should maintain its RCM at the port. To verify if both these objectives are met, the following two types of error are defined: E_{traj} is the deviation of the traced trajectory from the desired trajectory and E_{port} is the deviation of the entry point of the end link from the port. As the specified port position should ideally intersect the end link, the E_{port} can be formulated as the difference of the end link length and sum of distances of port from $\mathbf{X}_{elb}$ and $\mathbf{X}_{end}$.

$$E_{traj} = \left\|\mathbf{X}_{end} - \mathbf{X}_{end}^{des}\right\| \tag{8}$$

$$E_{port} = \mathrm{k}\mathbf{X}_{elb} - \mathbf{X}_p\mathrm{k} + \mathrm{k}\mathbf{X}_{end} - \mathbf{X}_p\mathrm{k} - \mathrm{k}\mathbf{X}_{elb} - \mathbf{X}_{end}\mathrm{k} \tag{9}$$

IV. Results

The proposed motion control algorithm was verified through simulation for both planar and 3-dimensional trajectories. Trajectories used for validation were obtained from hand motion as published in LIBRAS [25] and Auslan [26] signs database. LIBRAS movement dataset contains 15 types of hand movements with 24 instances for each type. Planar curves in the database were obtained from videos of hand movements in the Brazilian sign language Libras performed by different persons. Motion data from the first 10 instances of each class were used for this paper. The 3D trajectories, as obtained from the Auslan database consists of samples of signs from the Australian sign language captured using a Nintendo PowerGlove. The data was collected in different sessions from 5 different signers, out of which single session data (each consisting of 92 different signs) from 3 signers is used here. As only the trajectory of hand motion was required, only the hand positions in 3D and 2D cartesian space were used. The link lengths of the arm were assumed as $\begin{bmatrix} 20 & 22 & 10 \end{bmatrix}$ cm and the port was assumed to be positioned at $\begin{pmatrix} 3 & 5.2 & 1 \end{pmatrix}$. Samples of desired trajectories and traced trajectories are shown in Fig. 2 and Fig. 3. The error in traced trajectory and in maintenance of RCM at the port position as calculated from (8) and (9) are shown in Table II.

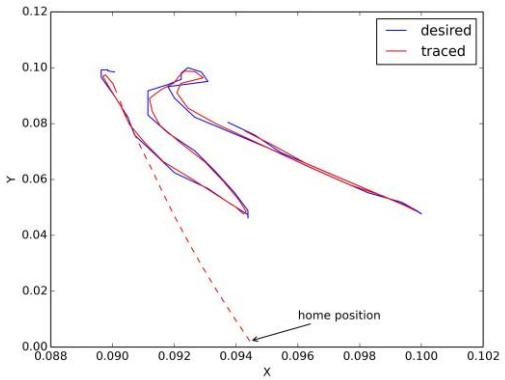

(a)

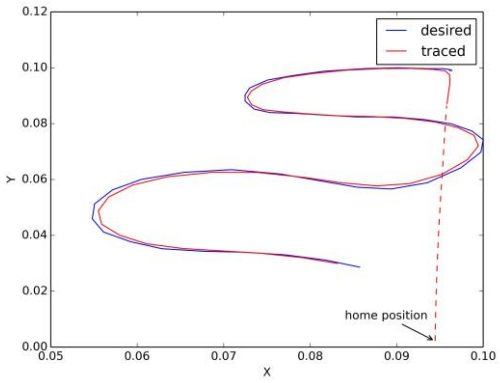

(b)

Fig. 2. Trajectories for (a) Class 3 and (b) Class 13 of hand movements from the LIBRAS dataset

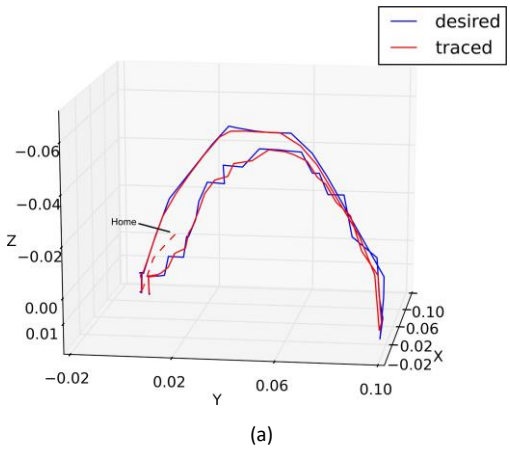

(a)

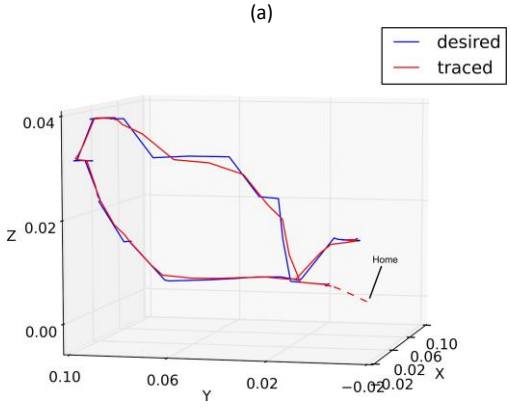

(b)

Fig. 3. Trajectories from Auslan dataset for the sign of (a) 'drink' given by Adam and (b) 'Cold' given by John in first session.

Table II

MEAN ERROR FOR TRAJECTORY TRACKING E_{traj} FOR EACH TYPE OF TRAJECTORY. THE MEAN ABSOLUTE E_{port} OBTAINED WAS ~0 $(< 10^{-15} cm)$ FOR ALL INSTANCES. HERE, μ IS THE MEAN AND σ IS THE STANDARD DEVIATION.

Trajectory	$E_{traj}\ (cm)$ $\mu \pm \sigma$
LIBRAS 1	8.5E-03±0.0043
LIBRAS 2	5.3E-03±0.0028
LIBRAS 3	6.2E-03±0.0038
LIBRAS 4	3.2E-03±0.0017
LIBRAS 5	3.2E-03±0.0019
LIBRAS 6	4.8E-03±0.0022
LIBRAS 7	1.7E-03±0.0011
LIBRAS 8	1.7E-03±0.0011
LIBRAS 9	1.2E-03±0.0009
LIBRAS 10	4.6E-03±0.0035
LIBRAS 11	4.2E-03±0.0028
LIBRAS 12	4.3E-03±0.0023
LIBRAS 13	4.0E-03±0.0017
LIBRAS 14	3.3E-03±0.0017
LIBRAS 15	3.7E-03±0.0020
Auslan (Adam)	8.6E-03±0.0136
Auslan (Andrew)	5.8E-03±0.0088
Auslan (John)	7.5E-03±0.0089

As can be observed from the Table II, errors in trajectory tracking and RCM maintenance at the port are sufficiently low, mean of E_{traj} being of the order of 10^{-3} and mean of absolute of E_{port} being negligible. This verifies that following the proposed motion control algorithm, a GARA can efficiently perform minimally invasive operations.

V. Conclusions

General articulated robotic arms are easily available, easier to install and maintain as compared to specially designed minimally invasive surgical robotic arms. Hence, such an arm that can switch to minimally invasive operation, can lend added functionality to an operational manipulator. This work hypothesizes that a motion control algorithm would suffice the aforementioned objective and later proves it over a 6-DoF GARA by drawing trajectories of hand motion in simulation under minimally invasive constraints. The proposed motion control algorithm basically relies on a novel transformation function which relates the elbow and end-effector coordinates such that the port constraints are met. Though this transformation function has been verified on a single manipulator configuration, it is applicable to other articulated robotic arms also, given the constraints apply only to the end link.

As future prospects of this work, dynamics analysis can be performed to analyze the effect of working forces and torques on the motion. Thus further control equations can be derived to dynamically maintain the virtual minimally invasive constraints. Such an additional control structure can increase the reliability of the manipulator.

References

[1] M. Kroh, K. El-Hayek, S. Rosenblatt, B. Chand, P. Escobar, J. Kaouk, and S. Chalikonda, "First human surgery with a novel single-port robotic system: cholecystectomy using the da Vinci Single-Site platform." *Surgical endoscopy*, vol. 25, no. 11, pp. 3566–73, Nov. 2011.

[2] Y. A. Park, J. M. Kim, S. A. Kim, B. S. Min, N. K. Kim, S. K. Sohn, and K. Y. Lee, "Totally robotic surgery for rectal cancer: from splenic flexure to pelvic floor in one setup." *Surgical endoscopy*, vol. 24, no. 3, pp. 715–20, Mar. 2010.

[3] M. C. Bell, J. Torgerson, U. Seshadri-Kreaden, A. W. Suttle, and S. Hunt, "Comparison of outcomes and cost for endometrial cancer staging via traditional laparotomy, standard laparoscopy and robotic techniques." *Gynecologic oncology*, vol. 111, no. 3, pp. 407–11, Dec. 2008.

[4] L. G. Seamon, D. E. Cohn, M. S. Henretta, K. H. Kim, M. J. Carlson, G. S. Phillips, and J. M. Fowler, "Minimally invasive comprehensive surgical staging for endometrial cancer: Robotics or laparoscopy?" *Gynecologic oncology*, vol. 113, no. 1, pp. 36–41, Apr. 2009.

[5] R. E. Betcher, J. P. Chaney, P. R. Lacy, S. K. Otey, and D. J. Wood, "Analysis of postoperative pain in robotic versus traditional laparoscopic hysterectomy," *Journal of Robotic Surgery*, vol. 8, no. 1, pp. 35–41, Jul. 2013.

[6] M. Lum, D. C. Friedman, G. Sankaranarayanan, H. King, and K. Fodero, "The raven: Design and validation of a telesurgery system," *The International Journal of Robotics Research*, vol. 28, no. 9, pp. 1183–1197, 2009.

[7] K. Xu and N. Simaan, "Actuation compensation for flexible surgical snake-like robots with redundant remote actuation," in *Robotics and Automation, 2006. ICRA 2006. Proceedings 2006 IEEE International Conference on*. IEEE, 2006, pp. 4148–4154.

[8] J. A. Walter and K. J. Schulten, "Implementation of self-organizing neural networks for visuo-motor control of an industrial robot," *Neural Networks, IEEE Transactions on*, vol. 4, no. 1, pp. 86–96, 1993.

[9] F. Pierrot, V. Nabat, O. Company, S. Krut, and P. Poignet, "Optimal design of a 4-dof parallel manipulator: from academia to industry," *Robotics, IEEE Transactions on*, vol. 25, no. 2, pp. 213–224, 2009.

[10] R. Thomson and J. Robertson, "Industrial manipulator for placing articles in close proximity to adjacent articles," Patent US 4273506, 06 16, 1981.

[11] S. Gupta, S. T. Sarkar, and A. Kumar, "Design optimization of minimally invasive surgical robot," *Applied Soft Computing*, vol. 32, pp. 241 – 249, 2015. [Online]. Available: http://www.sciencedirect.com/science/article/pii/S1568494615001908

[12] C.-H. Kuo, J. S. Dai, and P. Dasgupta, "Kinematic design considerations for minimally invasive surgical robots: an overview," *The International Journal of Medical Robotics and Computer Assisted Surgery*, vol. 8, no. 2, pp. 127–145, 2012.

[13] S.-K. Kim, W.-H. Shin, S.-Y. Ko, J. Kim, and D.-S. Kwon, "Design of a compact 5-dof surgical robot of a spherical mechanism: Cures," in *Advanced Intelligent Mechatronics, 2008. AIM 2008. IEEE/ASME International Conference on*. IEEE, 2008, pp. 990–995.

[14] G. Guthart and J. K. Salisbury Jr, "The intuitivetm telesurgery system: Overview and application." in *ICRA*, 2000, pp. 618–621.

[15] A. J. Madhani, G. Niemeyer, and J. K. Salisbury, "The black falcon: a teleoperated surgical instrument for minimally invasive surgery," in *Intelligent Robots and Systems, 1998. Proceedings., 1998 IEEE/RSJ International Conference on*, vol. 2. IEEE, 1998, pp. 936–944.

[16] M. J. Lum, J. Rosen, M. N. Sinanan, and B. Hannaford, "Optimization of a spherical mechanism for a minimally invasive surgical robot: theoretical and experimental approaches," *Biomedical Engineering, IEEE Transactions on*, vol. 53, no. 7, pp. 1440–1445, 2006.

[17] M. Lum, J. Rosen, M. N. Sinanan, and B. Hannaford, "Kinematic optimization of a spherical mechanism for a minimally invasive surgical robot," in *Robotics and Automation, 2004. Proceedings. ICRA'04. 2004 IEEE International Conference on*. IEEE, 2004, pp. 829–834.

[18] H. Kang and J. Wen, "Robotic assistants aid surgeons during minimally invasive procedures," *Engineering in Medicine and Biology Magazine, IEEE*, vol. 20, no. 1, pp. 94–104, 2001.

[19] J. Li, S. Wang, X. Wang, and C. He, "Optimization of a novel mechanism for a minimally invasive surgery robot," *The international journal of medical robotics and computer assisted surgery*, vol. 6, no. 1, pp. 83– 90, 2010.

[20] M. Michelin, E. Dombre, P. Poignet, F. Pierrot, and L. Eckert, "Path planning under a penetration point constraint for minimally invasive surgery," in *Intelligent Robots and Systems, 2002. IEEE/RSJ International Conference on*, vol. 2. IEEE, 2002, pp. 1475–1480.

[21] L. Wang and C. Chen, "A combined optimization method for solving the inverse kinematics problems of mechanical manipulators," *Robotics and Automation, IEEE Transactions on*, vol. 7, no. 4, 1991.

[22] S. Buss and J. Kim, "Selectively damped least squares for inverse kinematics," *Journal of Graphics, Gpu, and Game Tools*, 2005.

[23] I-Ming Chen and Guilin Yang, "Inverse kinematics for modular reconfigurable robots," in *Proceedings. 1998 IEEE International Conference on Robotics and Automation (Cat. No.98CH36146)*, vol. 2. IEEE, 1998, pp. 1647–1652.

[24] D. Whitney, "Resolved motion rate control of manipulators and human prostheses," *Man-Machine Systems, IEEE Transactions on*, 1969.

[25] D. B. Dias, R. C. B. Madeo, T. Rocha, H. H. Biscaro, and S. M. Peres, "Hand movement recognition for Brazilian Sign Language: A study using distance-based neural networks," in *2009 International Joint Conference on Neural Networks*. IEEE, Jun. 2009, pp. 697–704.

[26] M. Kadous, "Learning Comprehensible Descriptions of Multivariate Time Series," in *Machine Learning: Proceedings of the Sixteenth International Conference*, I. Bratko and S. Dzeroski, Eds. San Francisco, CA: Morgan Kaufmann Publishers.

[27] M. Lichman, "UCI machine learning repository," 2013, university of California, Irvine, School of Information and Computer Sciences.

[28] J. Denavit and R. S. Hartenberg, "A kinematic notation for lower-pair mechanisms based on matrices." *Trans. of the ASME. Journal of Applied Mechanics*, 1955.

[29] C. Lee, "Robot Arm Kinematics, Dynamics, and Control," *Computer*, vol. 15, no. 12, pp. 62–80, Dec. 1982.

[30] Y. Umetani and K. Yoshida, "Resolved motion rate control of space manipulators with generalized Jacobian matrix," *Robotics and Automation, IEEE Transactions on*, vol. 5, no. 3, pp. 303–314, 1989.